Electronic Supplementary Material (ESI) for Nanoscale.

Supporting Information (SI)

Two-Dimensional Transition Metal Borides as High Activity and Selectivity Catalysts for Ammonia Synthesis

Haona Zhang, Shuhua Wang, Hao Wang, Baibiao Huang, Shuping Dong, Ying Dai,* and Wei Wei*

School of Physics, State Key Laboratory of Crystal Materials, Shandong University, Jinan 250100, China

* Corresponding authors: daiy60@sdu.edu.cn (Y. Dai), weiw@sdu.edu.cn (W. Wei)

COMPUTATIONAL METHODS

All the geometry optimization and electronic property calculations were performed by means of the spin-polarized density functional theory (DFT), using Vienna *ab initio* simulation package (VASP).[1,2] The generalized gradient approximation (GGA) with the Perdew–Burke–Ernzerhof (PBE)[3,4] formalism was applied to describe the exchange correlation functional. In addition, the projector-augmented wave (PAW) method[5,6] was used to treat the core−valence interactions with a kinetic cutoff energy of 550 eV for the plane wave basis set. Considering the van der Waals interactions (vdW), the DFT–D2 by Grimme was carried out in this work.[7] The coverage tolerances for total energy and force were set to 10^{-5} eV and 0.01 eV/Å, respectively. The Monkhorst–Pack *k*-point meshes of 3×3×1 and 5×5×1 were implemented in geometry optimization and electronic self-consistence for a 2×3 supercell of TMB_2 system, respectively. In order to avoid the interactions between periodic images, a vacuum space of 20 Å was applied along the *z* axis. The thermal stability of the TMB_2 was evaluated by *ab initio* molecular dynamics (AIMD) simulations at 700 K for 5 ps with a time step of 1 fs. The transition states and kinetic energy barriers were calculated by the climbing-image nudged elastic band (CI-NEB) method.[8]

The computational hydrogen electrode (CHE) model[9,10] was applied to compute the Gibbs free energy change (ΔG) for each elemental step in the NRR process, which can be obtained from the following equation

$$\Delta G = \Delta E + \Delta E_{ZPE} - T\Delta S + eU + \Delta G_{pH}$$

where ΔE is the electronic energy difference between the product and reactant of each

elemental step in NRR process, ΔE_{ZPE} and ΔS are the corresponding changes in zero-point energy and entropy, respectively, obtained from frequency calculations at T = 298.15 K. The entropy of gas molecules (N_2 and NH_3) was taken from standard values. e is the number of transferred electrons and U stands for the applied electrode potential. ΔG_{pH} is the correction of pH, which can be expressed by

$$\Delta G_{pH} = \ln 10 \times k_B T \times pH$$

where k_B is the Boltzmann constant and the value of pH is set to zero in this work.

To ensure every protonation step exothermic, an additional voltage should be applied, which is defined as the limiting potential (U_L) that can be obtained from the free energy change in the potential-determining step (PDS)

$$U_L = -\Delta G_{max}/e$$

MICROKINETIC MODELING

The elementary reactions of ammonia synthesis on the ReB_2 are considered

$$N_2\ (g) + 2^* \leftrightarrow {}^{**}N_2 \quad \text{(R1)}$$

$$H_2\ (g) + 2^* \leftrightarrow 2H^* \quad \text{(R2)}$$

$${}^{**}N_2 + H^* \leftrightarrow {}^{**}N_2H + * \quad \text{(R3)}$$

$${}^{**}N_2H + H^* \leftrightarrow {}^{**}N_2H_2 + * \quad \text{(R4)}$$

$${}^{**}N_2H_2 + H^* \leftrightarrow {}^{**}N_2H_3 + * \quad \text{(R5)}$$

$${}^{**}N_2H_3 + H^* \leftrightarrow 2^*NH_2 + * \quad \text{(R6)}$$

$$^*NH_2 + H^* \leftrightarrow {}^*NH_3 + * \quad \text{(R7)}$$

$$^*NH_3 \leftrightarrow NH_3\ (g) + * \quad \text{(R8)}$$

where * represents a metal active site. Considering that N_2 adsorption on ReB_2 in side-on pattern occupies two reaction sites, and thus is denoted as $^{**}N_2$. The rate of each elementary step can be written as

$$r_1 = k_1 p_{N_2} \theta_*^2 - k_{-1} \theta_{^{**}N_2} \#(1)$$

$$r_2 = k_2 p_{H_2} \theta_*^2 - k_{-2} \theta_{^*H}^2 \#(2)$$

$$r_3 = k_3 \theta_{^{**}N_2} \theta_{^*H} - k_{-3} \theta_{^{**}N_2H} \theta_* \#(3)$$

$$r_4 = k_4 \theta_{^{**}N_2H} \theta_{^*H} - k_{-4} \theta_{^{**}N_2H_2} \theta_* \#(4)$$

$$r_5 = k_5 \theta_{^{**}N_2H_2} \theta_{^*H} - k_{-5} \theta_{^{**}N_2H_3} \theta_* \#(5)$$

$$r_6 = k_6 \theta_{^{**}N_2H_3} \theta_{^*H} - k_{-6} \theta_{^*NH_2}^2 \theta_* \#(6)$$

$$r_7 = k_7 \theta_{^*NH_2} \theta_{^*H} - k_{-7} \theta_{^*NH_3} \theta_* \#(7)$$

$$r_8 = k_8 \theta_{^*NH_3} - k_{-8} p_{NH_3} \theta_* \#(8)$$

where k_i is the rate constant for step i, p denotes the partial pressure of gas N_2 and NH_3, θ denotes the coverage of the adsorbed species (N_xH_y). Our kinetic barrier calculation shows that the step R_4 is the rate-determining step (RDS), therefore, under the quasi-equilibrium approximation (QEA),[11–13] the rates of all the other steps equal to zero ($r_1 = r_2 = r_3 = r_5 = r_6 = r_7 = 0$). Hence, the coverage of reaction species can be obtained

$$\theta_{^{**}N_2} = K_1 p_{N_2} \theta_*^2 \#(9)$$

$$\theta_{^*H} = \sqrt{K_2 p_{H_2} \theta_*^2} \#(10)$$

$$\theta_{^{**}N_2H} = K_3 K_1 \sqrt{K_2 p_{H_2}} p_{N_2} \theta_*^2 \#(11)$$

$$\theta_{^{**}N_2H_2} = \frac{p_{NH_3}^2 \theta_*^2}{K_8^2 K_7^2 K_6 K_5 K_2^2 P_{H_2}^2} \#(12)$$

$$\theta_{**N_2H_3} = \frac{p_{NH_3}^2 \theta_*^2}{K_8^2 K_7^2 K_6 \sqrt{K_2 p_{H_2}}^3} \#(13)$$

$$\theta_{*NH_2} = \frac{p_{NH_3} \theta_*}{K_8 K_7 \sqrt{K_2 p_{H_2}}} \#(14)$$

$$\theta_{*NH_3} = \frac{p_{NH_3} \theta_*}{K_8} \#(15)$$

where $K_i = k_i / k_{-i}$ is the equilibrium constant for step i, which can be expressed by

$$K_i = e^{\frac{-\Delta G_i}{k_B T}} \#(16)$$

$$k_i = \frac{k_B T}{h} e^{\frac{-\Delta G_{TS}}{k_B T}} \#(17)$$

where ΔG_i and ΔG_{TS} are free energies of reaction and activation, respectively. k_B is Boltzmann constant; h is Planck constant. The sum of coverage of all the reaction species equals to one

$$\sum_i \theta_i = 1 \#(18)$$

Combining Equations (9)–(18), a quadratic equation on θ_* can be solved analytically with the conversion ratio of NH_3 fixed at 10%.[13] Then, the rate of slow step R_3 can be obtained.

Table S1. Structure parameters (a and b), area of the optimized unit cell (S_0), and $\partial^2 E_{total}/\partial\varepsilon^2$ of TMB_2.

	a (Å)	b (Å)	S_0 (Å^2)	$\partial^2 E_{total}/\partial\varepsilon^2$
TiB_2	4.55	2.99	13.62	85.22
VB_2	4.54	2.86	12.99	94.65
CrB_2	4.48	2.82	12.62	82.71
MnB_2	4.52	2.69	12.18	100.81
FeB_2	4.51	2.64	11.89	122.72
CoB_2	4.68	2.51	11.76	146.96
NbB_2	4.58	2.93	13.43	97.05
MoB_2	4.65	2.84	13.22	109.05
TcB_2	4.51	2.87	12.94	106.64
RuB_2	4.50	2.84	12.77	131.97
WB_2	4.64	2.82	13.06	124.86
ReB_2	4.65	2.77	12.89	136.47
OsB_2	4.56	2.81	12.78	145.58

Table S2. Total energy of TMB_2 (E_{TMB2}), energy of single TM atom (E_{TM}) and cohesive energy (E_{coh}).

	E_{TMB2} (eV)	E_{TM} (eV)	E_{coh} (eV)
TiB_2	–40.95	–2.30	5.84
VB_2	–42.67	–3.58	5.70
CrB_2	–43.05	–5.44	5.14
MnB_2	–42.82	–5.11	5.21
FeB_2	–41.50	–3.30	5.60
CoB_2	–39.10	–1.72	5.72
NbB_2	–45.46	–3.21	6.29
MoB_2	–46.52	–4.59	6.00
TcB_2	–45.92	–3.39	6.30
RuB_2	–43.91	–2.47	6.27
WB_2	–51.06	–4.54	6.78
ReB_2	–50.40	–4.61	6.64
OsB_2	–48.37	–2.93	6.86

Table S3. Total energy of TMB_2 with (E) and without N_2 adsorption (E_{*N2}); zero-point energy (E_{ZPE}) and entropy (TS) for NRR on TMB_2 monolayer with N_2 end-on adsorption.

	E	E_{*N2}	E_{ZPE}	TS	ΔG_{*N2}
VB_2	–256.04	–274.20	0.19	0.19	–1.08
CrB_2	–258.27	–276.23	0.19	0.25	–0.93
MnB_2	–256.93	–274.66	0.20	0.18	–0.62
FeB_2	–248.92	–266.62	0.20	0.19	–0.61
CoB_2	–234.49	–252.23	0.22	0.14	–0.59
NbB_2	–272.67	–290.27	0.19	0.20	–0.54
MoB_2	–278.99	–296.69	0.19	0.20	–0.61
TcB_2	–275.40	–293.15	0.19	0.23	–0.72
RuB_2	–263.30	–280.87	0.21	0.16	–0.45
WB_2	–306.33	–324.54	0.20	0.20	–1.13
ReB_2	–302.03	–319.96	0.20	0.16	–0.80
OsB_2	–289.98	–307.77	0.21	0.15	–0.64

Table S4. Total energy of TMB_2 with (E) and without N_2 adsorption (E_{*N2}); zero-point energy (E_{ZPE}) and entropy (TS) for NRR on TMB_2 monolayer with N_2 side-on adsorption.

	E	E_{*N2}	E_{ZPE}	TS	ΔG_{*N2}
TiB_2	–245.65	–263.99	0.20	0.11	–1.17
VB_2	–256.04	–274.81	0.20	0.11	–1.60
CrB_2	–258.27	–277.02	0.19	0.13	–1.61
MnB_2	–256.93	–274.62	0.19	0.13	–0.55
FeB_2	–248.92	–266.36	0.18	0.16	–0.34
NbB_2	–272.67	–290.92	0.19	0.13	–1.11
MoB_2	–278.99	–296.96	0.19	0.13	–0.82
TcB_2	–275.40	–293.11	0.18	0.16	–0.62
RuB_2	–263.30	–280.50	0.16	0.23	–0.18
WB_2	–306.33	–324.91	0.19	0.12	–1.42
ReB_2	–302.03	–319.80	0.18	0.13	–0.64
OsB_2	–289.98	–307.27	0.17	0.16	–0.20

Table S5. Total energy (E_{tot}), zero-point energy (E_{ZPE}) and entropy (TS) of intermediates for NRR on CrB_2 along mix pathway.

	E_{tot}	E_{ZPE}	TS	G
$*N_2$	–276.23	0.19	0.25	–276.29
*N-NH	–279.83	0.47	0.14	–279.50
*NH-NH	–283.37	0.76	0.19	–282.80
$*NH\text{-}NH_2$	–287.27	1.12	0.25	–286.40
$*NH_2\text{-}NH_2$	–293.94	1.40	0.16	–292.70
$*NH_2\text{-}NH_3$	–296.44	1.71	0.25	–294.98
$*NH_2$	–275.68	0.47	0.14	–275.35
$*NH_3$	–279.20	1.00	0.19	–278.39

Table S6. Total energy (E_{tot}), zero-point energy (E_{ZPE}) and entropy (TS) of intermediates for NRR on ReB_2 along distal pathway.

	E_{tot}	E_{ZPE}	TS	G
$*N_2$	–319.96	0.20	0.16	–319.92
*N-NH	–323.33	0.47	0.17	–323.03
$*N\text{-}NH_2$	–327.26	0.79	0.21	–326.68
$*N\text{-}NH_3$	–332.43	1.11	0.19	–331.51
*N	–310.27	0.07	0.09	–310.29
*NH	–315.55	0.34	0.11	–315.32
$*NH_2$	–319.91	0.66	0.12	–319.37
$*NH_3$	–323.77	1.03	0.17	–322.91

Table S7. Total energy (E_{tot}), zero-point energy (E_{ZPE}) and entropy (TS) of intermediates for NRR on ReB_2 along mix pathway.

	E_{tot}	E_{ZPE}	TS	G
*N_2	–319.96	0.20	0.16	–319.92
*N-NH	–323.33	0.47	0.17	–323.03
*NH-NH	–327.05	0.83	0.17	–326.39
*NH-NH_2	–332.04	1.15	0.15	–331.04
*NH_2-NH_2	–337.19	1.35	0.21	–336.05
*NH_2-NH_3	–341.26	1.71	0.22	–339.77
*NH_2	–319.91	0.66	0.12	–319.37
*NH_3	–323.77	1.03	0.17	–322.91

Table S8. Total energy (E_{tot}), zero-point energy (E_{ZPE}) and entropy (TS) of intermediates for NRR on OsB_2 along distal pathway.

	E_{tot}	E_{ZPE}	TS	G
$*N_2$	–307.77	0.21	0.15	–307.71
*N-NH	–310.60	0.49	0.15	–310.26
$*N\text{-}NH_2$	–314.26	0.80	0.21	–313.67
$*N\text{-}NH_3$	–319.74	1.12	0.17	–318.79
*N	–298.44	0.08	0.04	–298.40
*NH	–302.67	0.35	0.08	–302.40
$*NH_2$	–307.24	0.68	0.11	–306.67
$*NH_3$	–311.20	1.03	0.13	–310.30

Table S9. Total energy (E_{tot}), zero-point energy (E_{ZPE}) and entropy (TS) of intermediates for NRR on CrB_2 along enzymatic pathway.

	E_{tot}	E_{ZPE}	TS	G
$*N_2$	–277.02	0.19	0.13	–276.96
*N-NH	–279.83	0.47	0.14	–279.50
*NH-NH	–283.37	0.76	0.19	–282.80
$*NH\text{-}NH_2$	–287.27	1.12	0.25	–286.40
$*NH_2\text{-}NH_2$	–293.94	1.40	0.16	–292.70
$*NH_2\text{-}NH_3$	–296.44	1.71	0.25	–294.98
$*NH_2$	–275.68	0.47	0.14	–275.35
$*NH_3$	–279.20	1.00	0.19	–278.39

Table S10. Total energy (E_{tot}), zero-point energy (E_{ZPE}) and entropy (TS) of intermediates for NRR on MnB_2 along enzymatic pathway.

	E_{tot}	E_{ZPE}	TS	G
*N_2	–274.62	0.19	0.13	–274.56
*N-NH	–277.80	0.48	0.12	–277.44
*NH-NH	–281.71	0.80	0.14	–281.05
*NH-NH_2	–285.64	1.13	0.16	–284.67
*NH_2-NH_2	–291.52	1.42	1.52	–291.62
*NH_2-NH_3	–295.22	1.72	0.26	–293.76
*NH_2	–274.28	0.70	0.08	–273.66
*NH_3	–277.71	1.02	0.17	–276.86

Table S11. Total energy (E_{tot}), zero-point energy (E_{ZPE}) and entropy (TS) of intermediates for NRR on FeB_2 along enzymatic pathway.

	E_{tot}	E_{ZPE}	TS	G
$*N_2$	–266.36	0.18	0.16	–266.34
*N-NH	–269.56	0.48	0.13	–269.21
*NH-NH	–273.62	0.81	0.12	–272.93
$*NH\text{-}NH_2$	–277.45	1.14	0.17	–276.48
$*NH_2\text{-}NH_2$	–282.02	1.36	0.20	–280.86
$*NH_2\text{-}NH_3$	–286.91	1.71	0.28	–285.48
$*NH_2$	–265.96	0.70	0.09	–265.35
$*NH_3$	–269.80	1.02	0.18	–268.96

Table S12. Total energy (E_{tot}), zero-point energy (E_{ZPE}) and entropy (TS) of intermediates for NRR on TcB_2 along enzymatic pathway.

	E_{tot}	E_{ZPE}	TS	G
$*N_2$	–293.11	0.18	0.16	–293.09
*N-NH	–296.26	0.47	0.13	–295.92
*NH-NH	–300.21	0.79	0.15	–299.57
$*NH\text{-}NH_2$	–304.20	1.13	0.17	–303.24
$*NH_2\text{-}NH_2$	–309.72	1.34	0.21	–308.59
$*NH_2\text{-}NH_3$	–313.79	1.71	0.27	–312.35
$*NH_2$	–292.94	0.70	0.08	–292.32
$*NH_3$	–296.17	1.01	0.18	–295.34

Table S13. Total energy (E_{tot}), zero-point energy (E_{ZPE}) and entropy (TS) of intermediates for NRR on RuB_2 along enzymatic pathway.

	E_{tot}	E_{ZPE}	TS	G
$*N_2$	–280.50	0.16	0.23	–280.57
*N-NH	–283.61	0.48	0.12	–283.25
*NH-NH	–287.65	0.80	0.14	–286.99
$*NH\text{-}NH_2$	–291.72	1.15	0.14	–290.71
$*NH_2\text{-}NH_2$	–296.25	1.31	0.24	–295.18
$*NH_2\text{-}NH_3$	–300.88	1.68	0.23	–299.43
$*NH_2$	–279.89	0.66	0.12	–279.35
$*NH_3$	–283.97	1.02	0.18	–283.13

Table S14. Total energy (E_{tot}), zero-point energy (E_{ZPE}) and entropy (TS) of intermediates for NRR on OsB_2 along enzymatic pathway.

	E_{tot}	E_{ZPE}	TS	G
*N_2	–307.27	0.17	0.16	–307.26
*N-NH	–310.92	0.49	0.11	–310.54
*NH-NH	–315.26	0.82	0.12	–314.56
*NH-NH_2	–319.01	1.16	0.15	–318.00
*NH_2-NH_2	–324.17	1.38	0.18	–322.97
*NH_2-NH_3	–328.37	1.72	0.21	–326.86
*NH_2	–307.10	0.71	0.09	–306.48
*NH_3	–311.20	1.03	0.13	–310.30

Table S15. Gibbs free energy change of *H at possible adsorption sites for 13 TMB_2.

	ΔG_{*H} (S1)	ΔG_{*H} (S2)	ΔG_{*H} (S3)	ΔG_{*H} (S4)
TiB_2	–0.23	0.27	/	/
VB_2	–0.72	/	–0.15	/
CrB_2	–0.60	–0.33	–0.26	/
MnB_2	–0.16	–0.17	–0.24	0.17
FeB_2	–0.09	–0.08	–0.07	/
CoB_2	–0.08	–0.24	–0.23	/
NbB_2	–1.03	–0.16	–0.21	/
MoB_2	–0.83	–0.27	–0.07	/
TcB_2	–0.39	0.09	–0.12	–0.16
RuB_2	–0.71	–0.33	–0.51	–0.56
WB_2	–0.99	/	–0.06	–0.06
ReB_2	–0.63	/	–0.03	–0.62
OsB_2	–0.33	/	0.05	–0.31

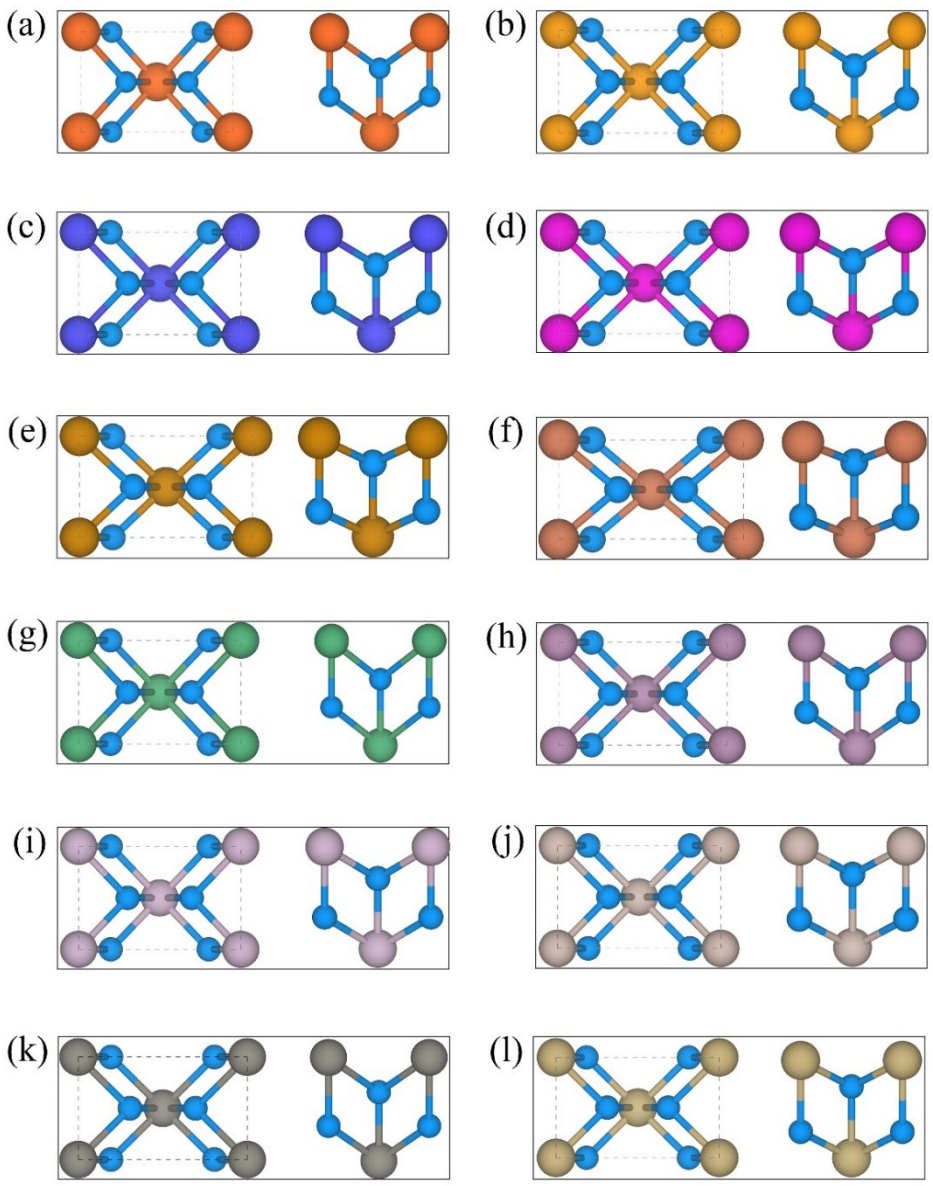

Fig. S1 Structure of (a) TiB_2, (b) VB_2, (c) CrB_2, (d) MnB_2, (e) FeB_2, (f) CoB_2, (g) NbB_2, (h) MoB_2, (i) TcB_2, (j) RuB_2, (k) WB_2, and (l) OsB_2, with rectangle marking the unit cell.

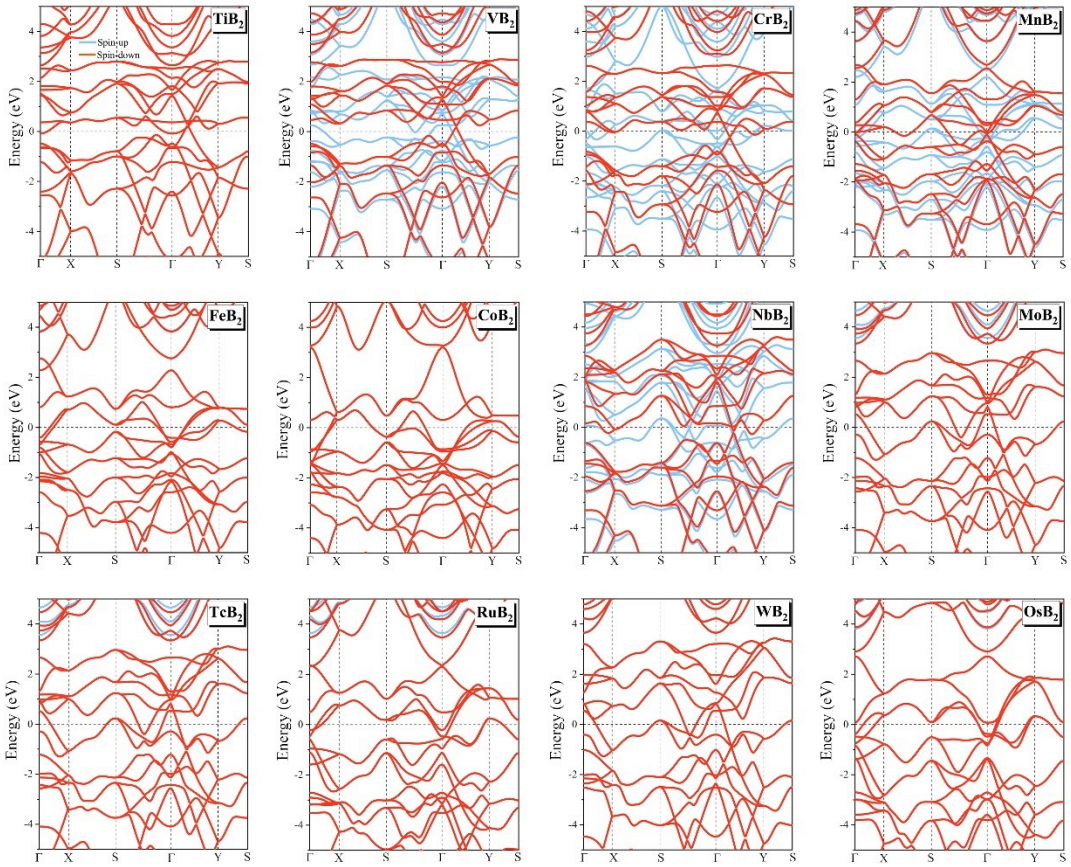

Fig. S2 Band structures of TMB_2. The Fermi level is set to zero.

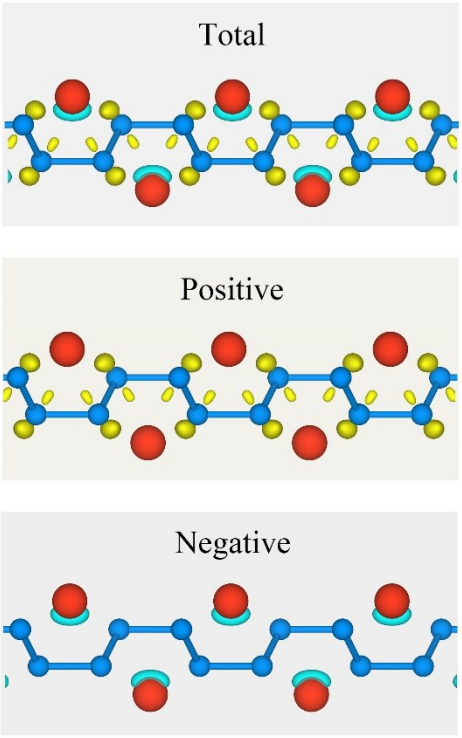

Fig. S3 Charge density difference with Re adsorption on borophene; yellow and cyan regions represent electron accumulation and depletion, respectively. The isosurface value is set to 0.03 e/Å^3.

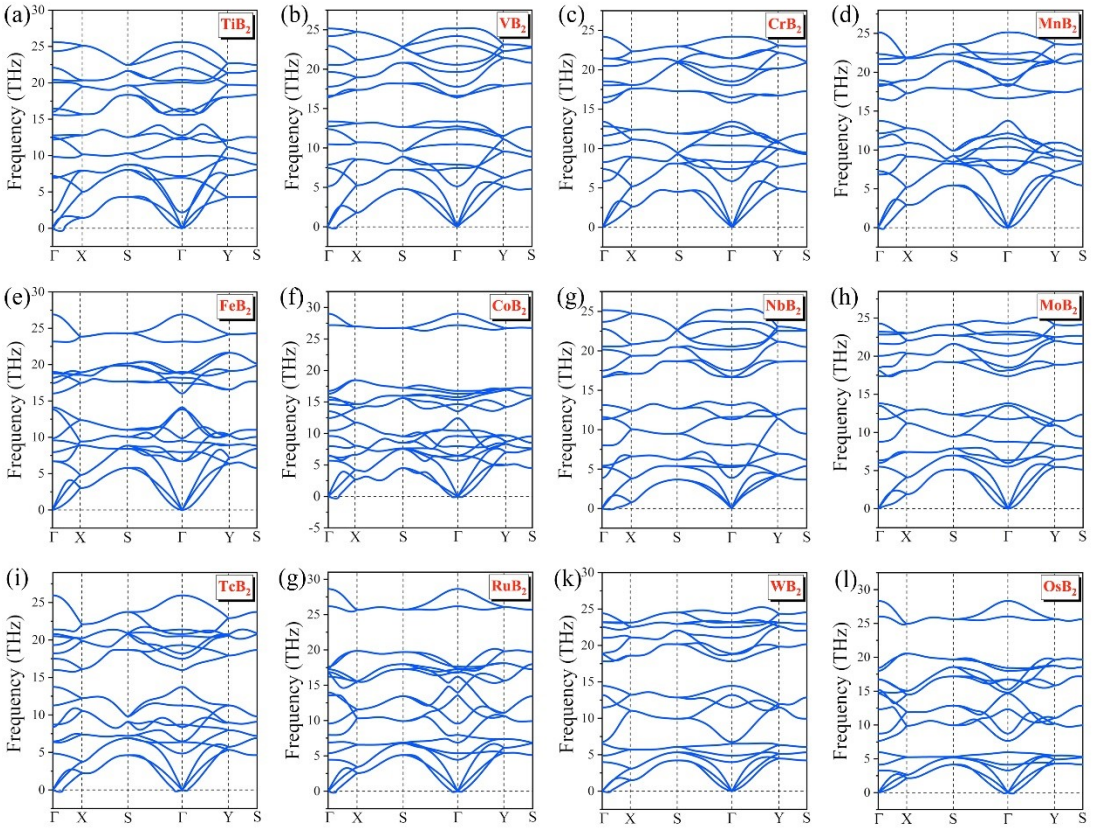

Fig. S4 Phonon spectrum of (a) TiB_2, (b) VB_2, (c) CrB_2, (d) MnB_2, (e) FeB_2, (f) CoB_2, (g) NbB_2, (h) MoB_2, (i) TcB_2, (j) RuB_2, (k) WB_2, and (l) OsB_2.

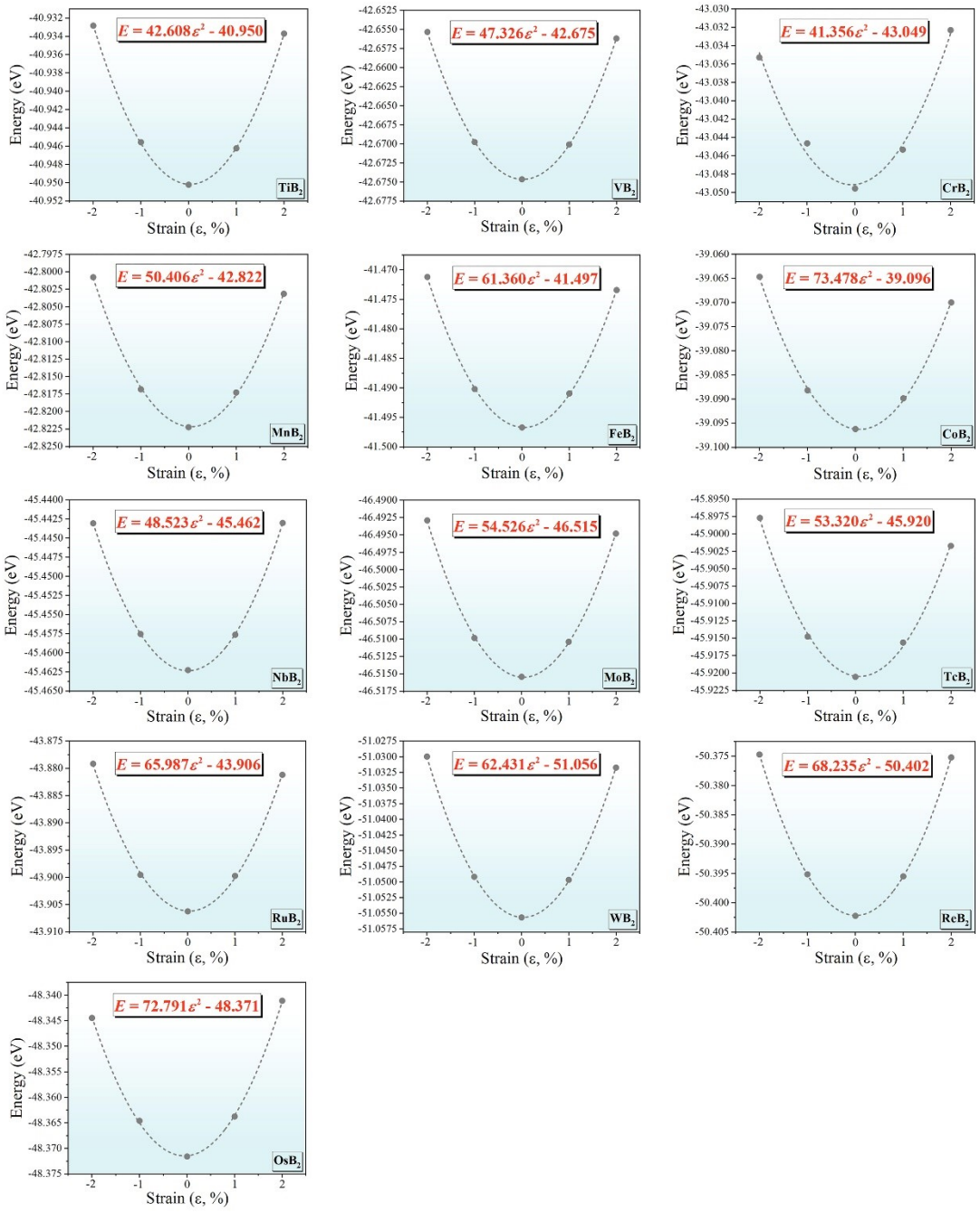

Fig. S5 Relationship between energy and strain along armchair directions.

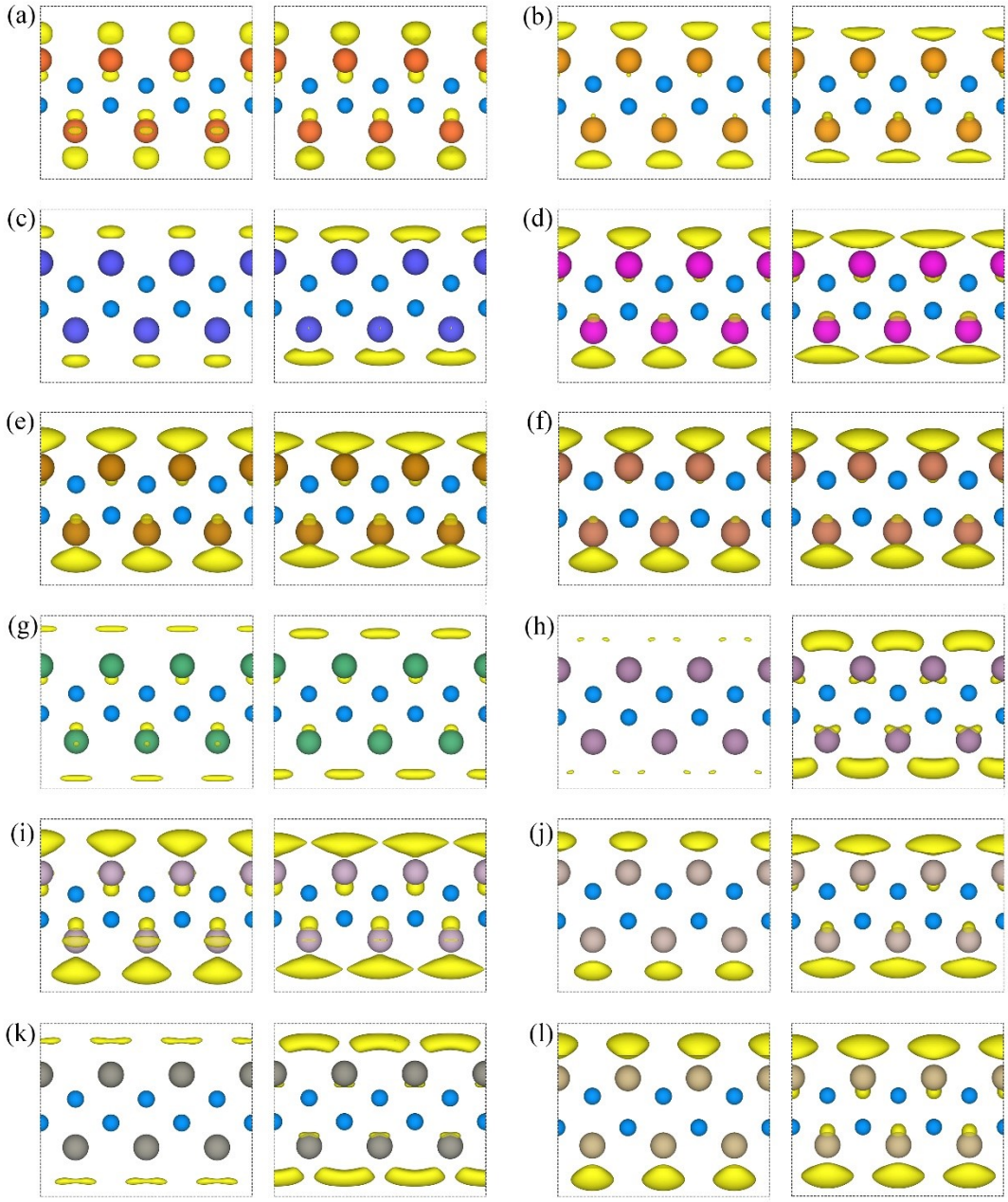

Fig. S6 Fukui functions of F^{+}(r) (left) and F^{-}(r) (right) of (a) TiB_2, (b) VB_2, (c) CrB_2, (d) MnB_2, (e) FeB_2, (f) CoB_2, (g) NbB_2, (h) MoB_2, (i) TcB_2, (j) RuB_2, (k) WB_2 and (l) OsB_2. The isosurface value is 0.001 e/Å^3.

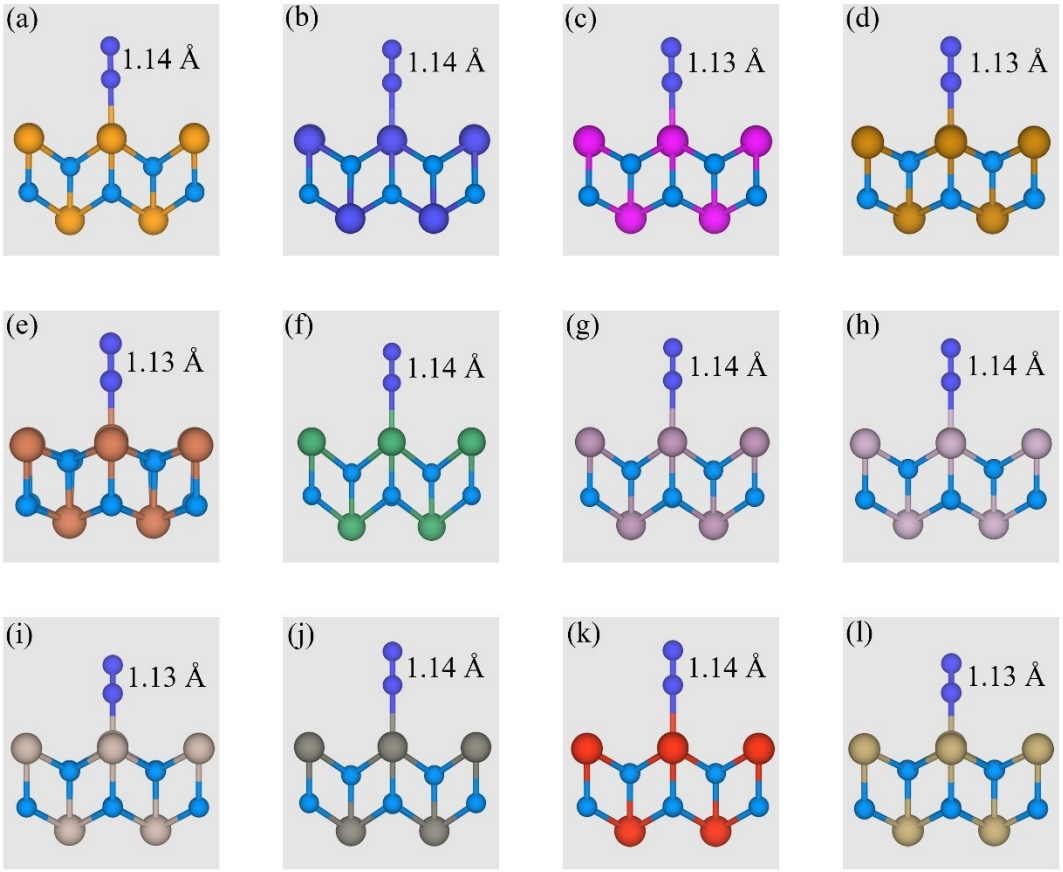

Fig. S7 Structures of N_2 end-on adsorption on (a) VB_2, (b) CrB_2, (c) MnB_2, (d) FeB_2, (e) CoB_2, (f) NbB_2, (g) MoB_2, (h) TcB_2, (i) RuB_2, (j) WB_2, (k) ReB_2 and (l) OsB_2.

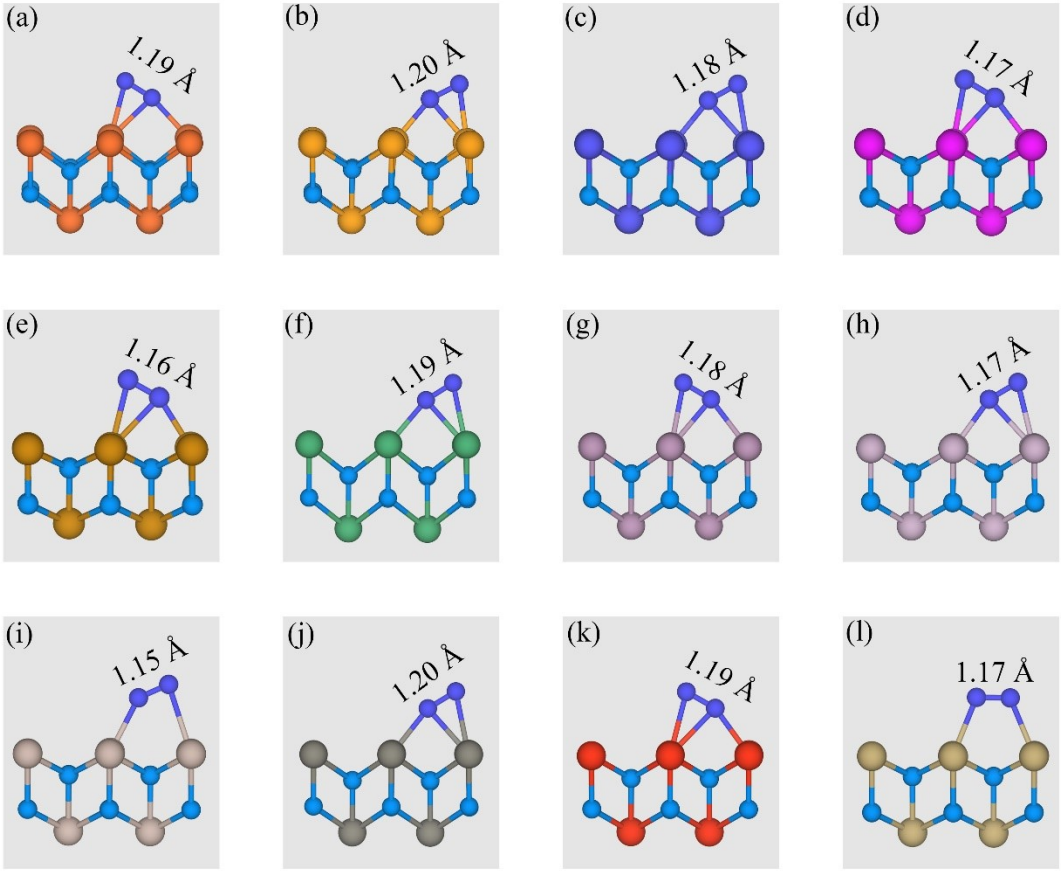

Fig. S8 Structures of N_2 side-on adsorption on (a) TiB_2, (b) VB_2, (c) CrB_2, (d) MnB_2, (e) FeB_2, (f) NbB_2, (g) MoB_2, (h) TcB_2, (i) RuB_2, (j) WB_2, (k) ReB_2 and (l) OsB_2.

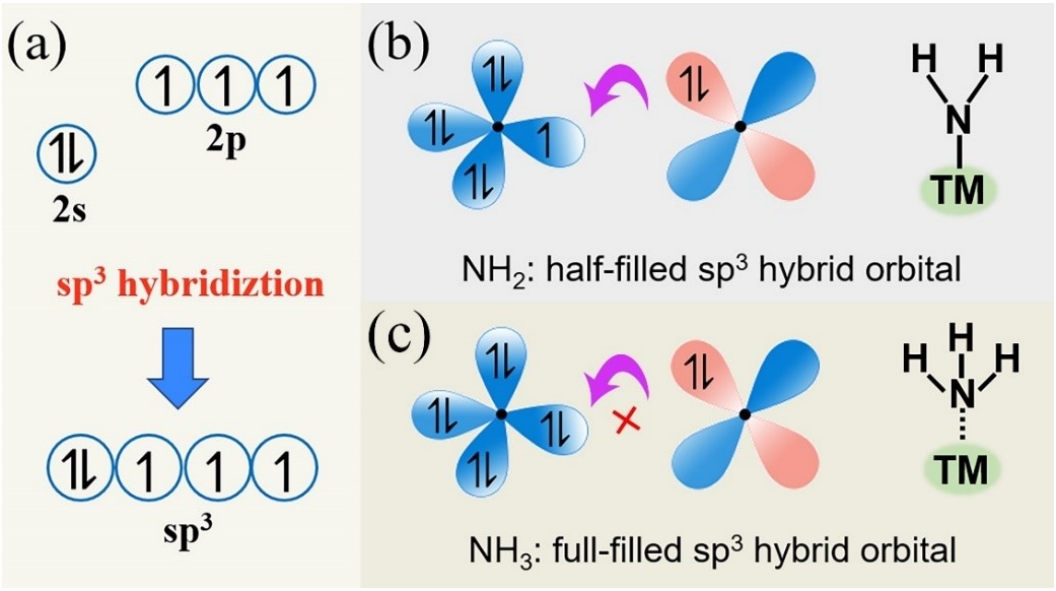

Fig. S9 Electronic configuration of (a) N with sp^3 hybridization, (b) $^*NH_2$ and (c) $^*NH_3$.

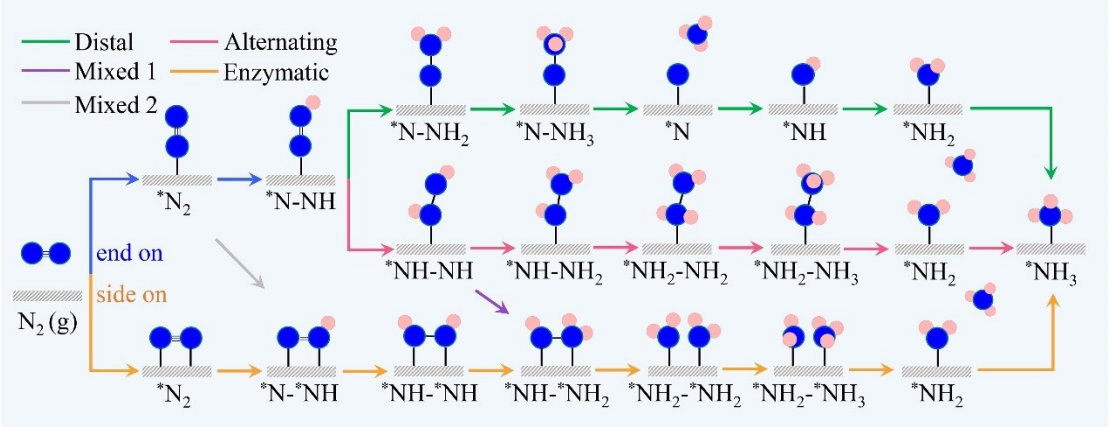

Fig. S10 Schematic of distal, alternating, enzymatic, and mixed mechanisms for N_2 reduction to NH_3. Blue and pink spheres represent N and H atoms, respectively.

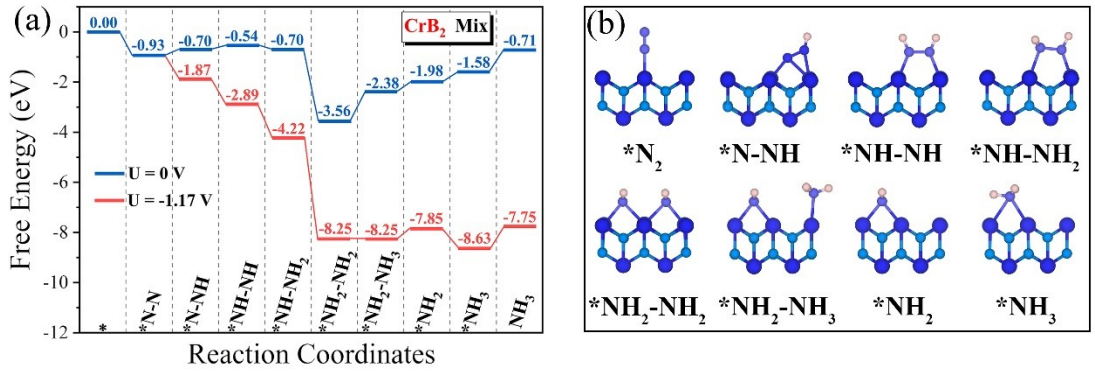

Fig. S11 (a) Gibbs free energy diagram for the NRR on CrB_2 at zero (blue line) and applied potential (red line) through mix mechanism. (b) Corresponding adsorption configurations of reaction intermediates.

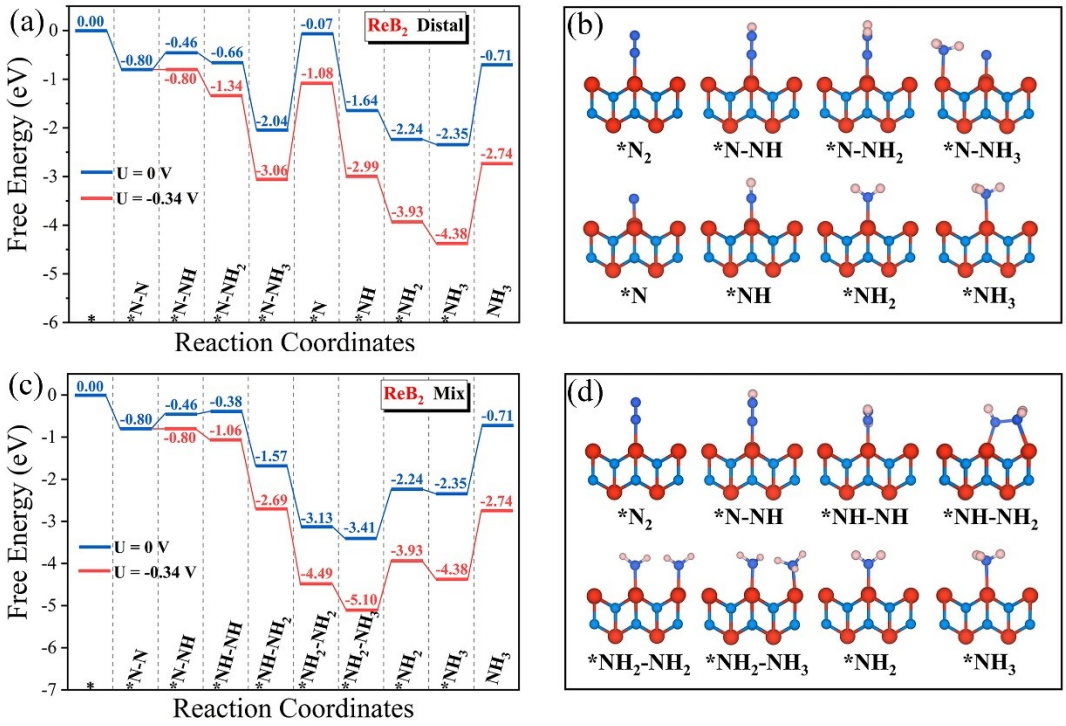

Fig. S12 Gibbs free energy diagram for NRR on ReB_2 at zero (blue line) and applied potential (red line) along (a) distal and (c) mix mechanisms. The corresponding adsorption configurations are displayed in (b) and (d).

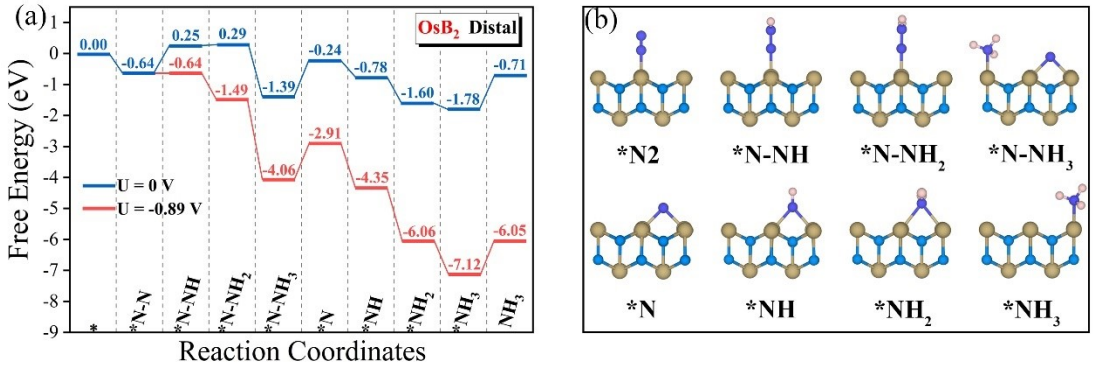

Fig. S13 (a) Gibbs free energy diagram for NRR on OsB_2 at zero (blue line) and applied potential (red line) through distal mechanism. (b) Corresponding adsorption configurations of reaction intermediates.

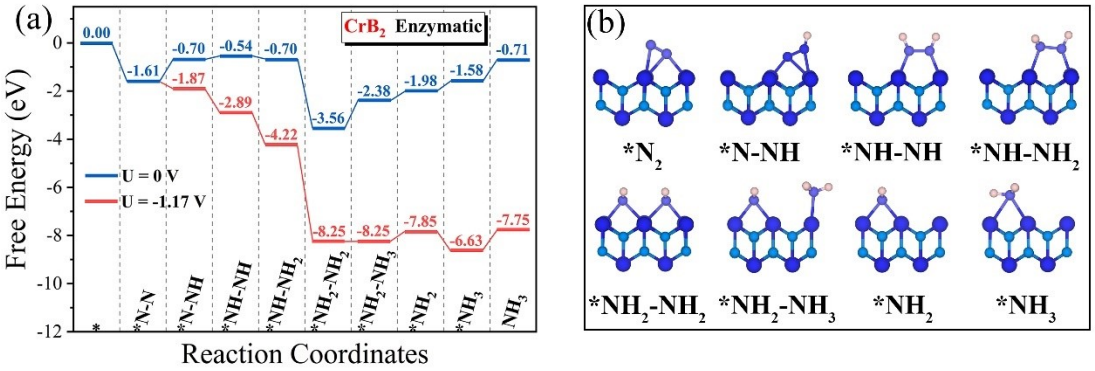

Fig. S14 (a) Gibbs free energy diagram for NRR on CrB_2 at zero (blue line) and applied potential (red line) through enzymatic mechanism. (b) Corresponding adsorption configurations of reaction intermediates.

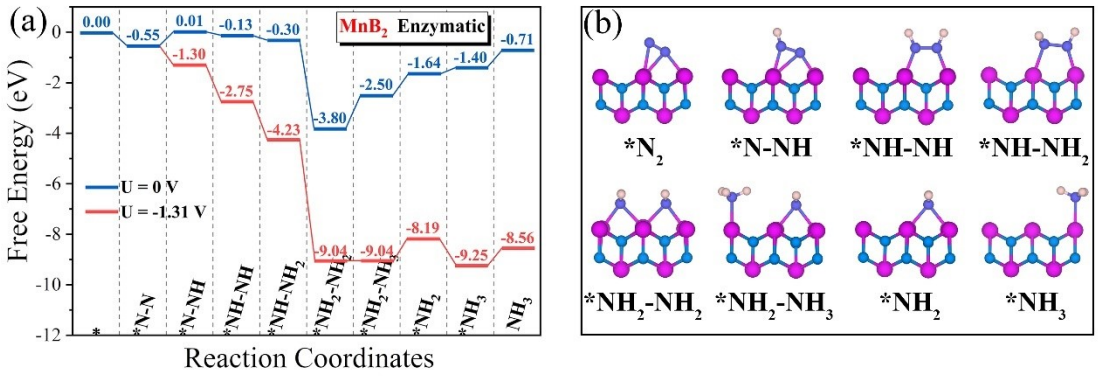

Fig. S15 (a) Gibbs free energy diagram for NRR on MnB_2 at zero (blue line) and applied potential (red line) through enzymatic mechanism. (b) Corresponding adsorption configurations of reaction intermediates.

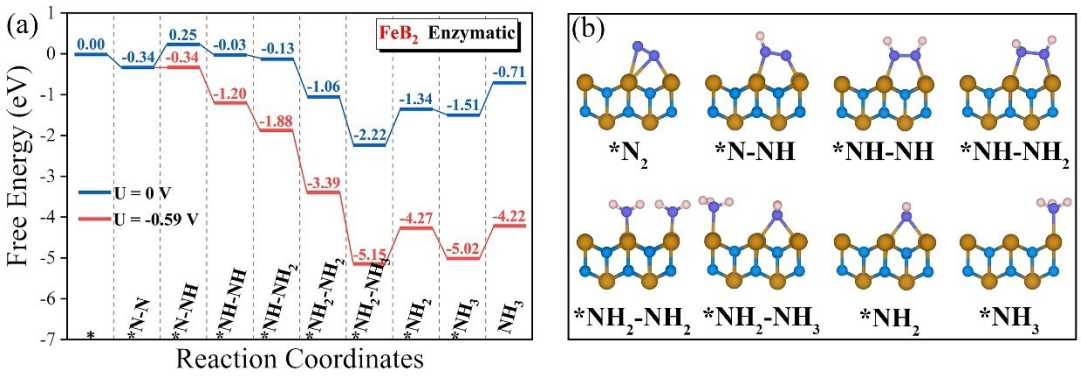

Fig. S16 (a) Gibbs free energy diagram for NRR on FeB_2 at zero (blue line) and applied potential (red line) through enzymatic mechanism. (b) Corresponding adsorption configurations of reaction intermediates.

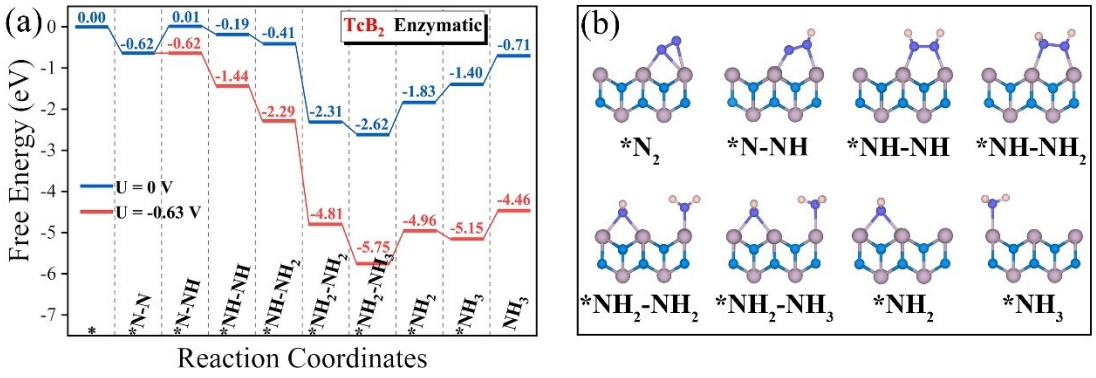

Fig. S17 (a) Gibbs free energy diagram for NRR on TcB_2 at zero (blue line) and applied potential (red line) through enzymatic mechanism. (b) Corresponding adsorption configurations of reaction intermediates.

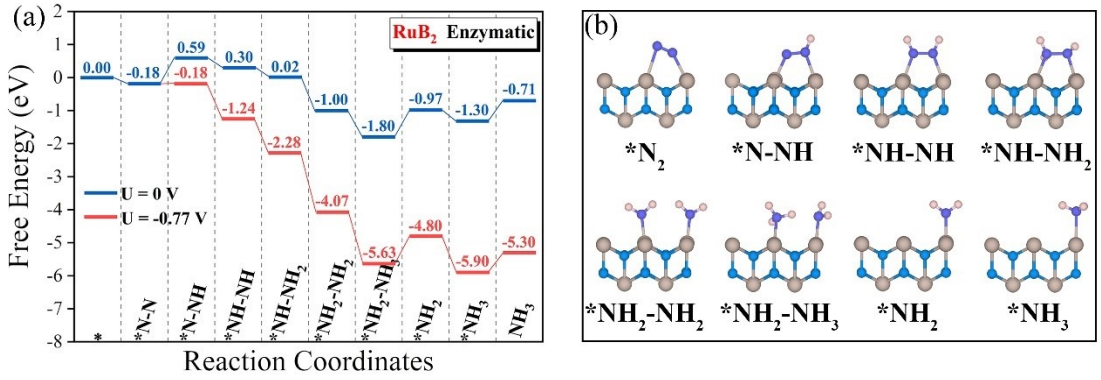

Fig. S18 (a) Gibbs free energy diagram for NRR on RuB_2 at zero (blue line) and applied potential (red line) through enzymatic mechanism. (b) Corresponding adsorption configurations of reaction intermediates.

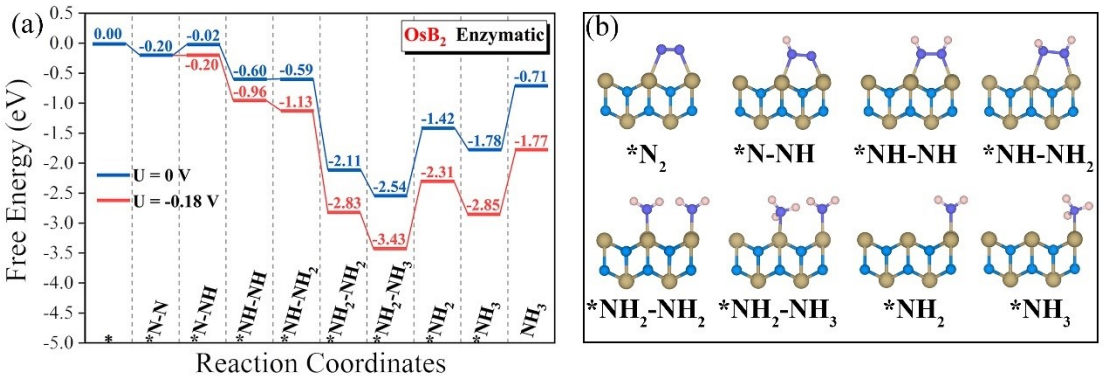

Fig. S19 (a) Gibbs free energy diagram for NRR on OsB_2 at zero (blue line) and applied potential (red line) through enzymatic mechanism. (b) Corresponding adsorption configurations of reaction intermediates.

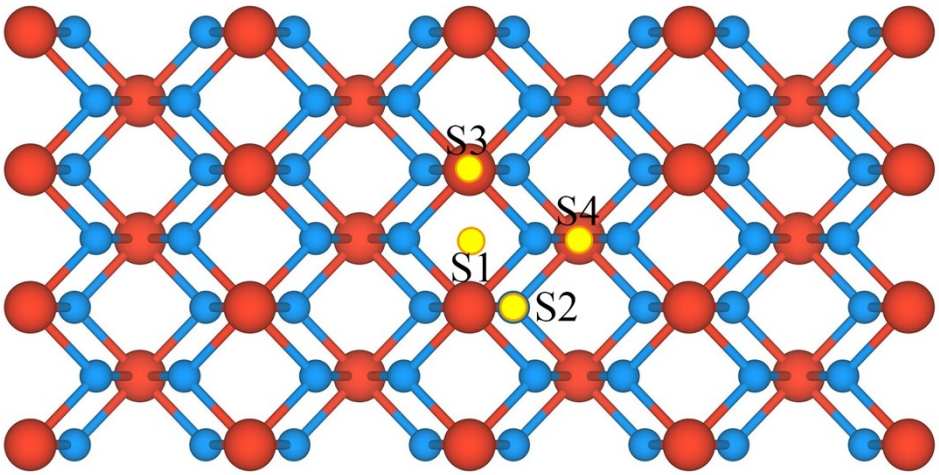

Fig. S20 Possible active sites for hydrogen adsorption.

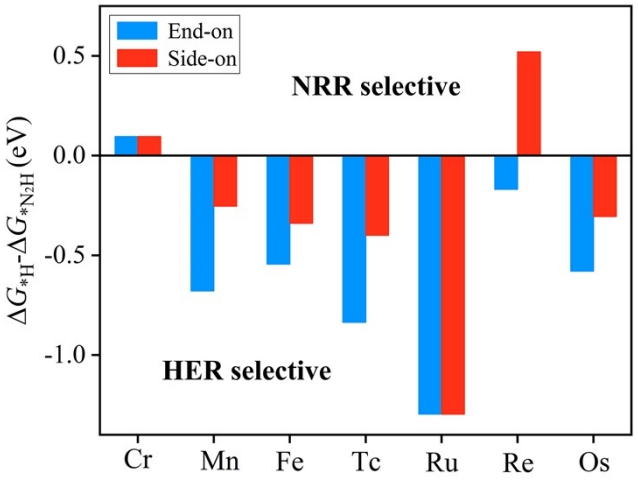

Fig. S21 Gibbs free energy difference of *H and *N_2H ($\Delta G_{*H} - \Delta G_{*N2H}$) on TMB_2 (TM = Cr, Mn, Fe, Tc, Ru, Re, Os).

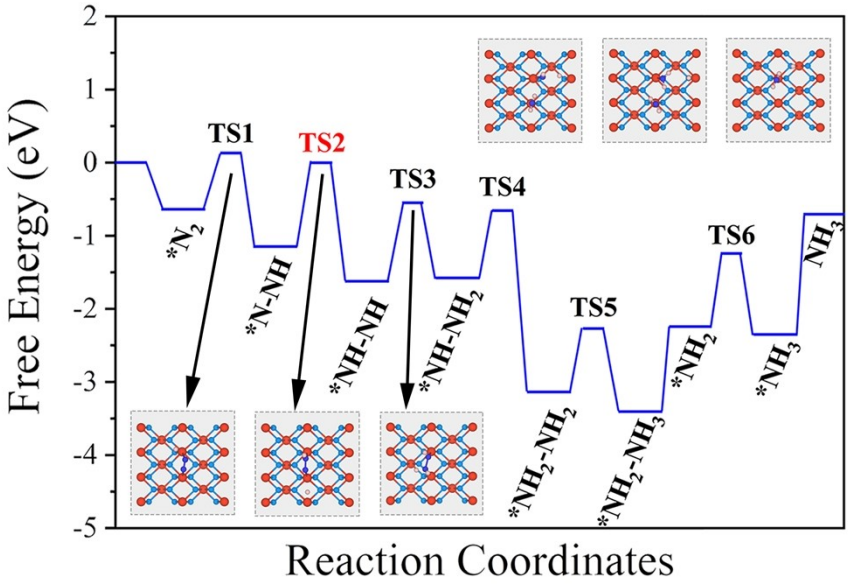

Fig. S22 Kinetic barriers for N_2 conversion to NH_3 on ReB_2, insets show the transition states. The H, B, N, and Re atoms are shown in pink, blue, cyan, and red colors, respectively.

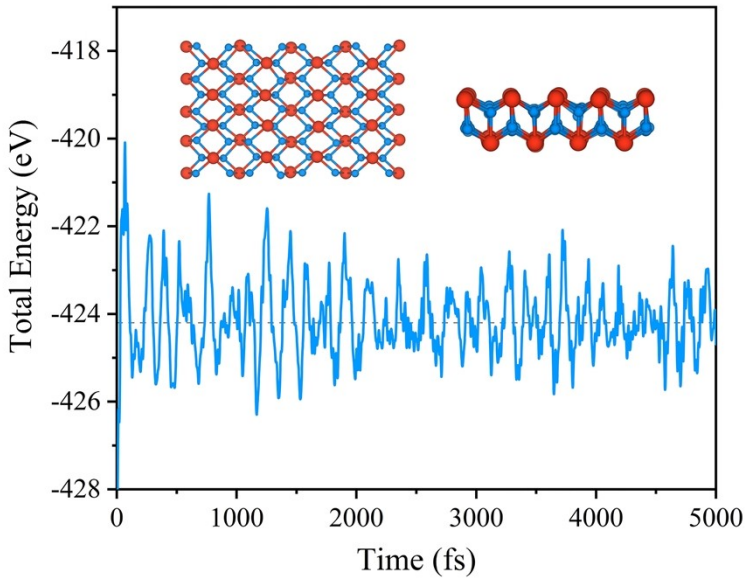

Fig. S23 AIMD simulations of ReB_2 at 700 K for 5 ps with a time step of 1 fs.

REFERENCE

1 G. Kresse and J. Furthmuller, *Phys. Rev. B*, 1996, **54**, 11169−11186.

2 G. Kresse and D. Joubert, *Phys. Rev. B*, 1999, **59**, 1758−1775.

3 J. P. Perdew and Y. Wang, *Phys. Rev. B*, 1992, **45**, 13244−13249.

4 J. P. Perdew, J. A. Chevary, S. H. Vosko, K. A. Jackson, M. R. Perderson, D. J. Singh and C. Fiolhais, *Phys. Rev. B*, 1992, **46**, 6671−6687.

5 P. E. Blochl, *Phys. Rev. B*, 1994, **50**, 17953−17979.

6 J. P. Perdew, K. Burke and M. Ernzerhof, *Phys. Rev. Lett.*, 1996, **77**, 3865–3868.

7 A. I. Liechtenstein, V. I. Anisimov and J. Zaanen, *Phys. Rev. B*, 1995, **52**, R5467−R5470.

8 G. Henkelman, B. P. Uberuaga and H. Jonsson, *J. Chem. Phys.*, 2000, **113**, 9901–9904.

9 J. K. Norskov, J. Rossmeisl, A. Logadottir, L. Lindqvist, J. R. Kitchin, T. Bligaard and H. Jonsson, *J. Phys. Chem. B*, 2004, **108**, 17886−17892.

10 H. Zhang, W. Wei, S. Wang, H. Wang, B. Huang and Y. Dai, *J. Mater. Chem. A*, 2021, **9**, 4082–4090.

11 H. Lynggaard, A. Andreasen, C. Stegelmann and P. Stoltze, *Prog. Surf. Sci.*, 2004, **77**, 71–137.

12 P. Stoltze, *Prog. Surf. Sci.*, 2000, **65**, 65–150.

13 J.-C. Liu, X.-L. Ma, Y. Li, Y. G. Wang, H. Xiao and J. Li, *Nat. Commun.*, 2018, **9**,

1610.